

# Exploring the Dark Energy Equation of State with JWST

Pei Wang<sup>1,2</sup>, Bing-Yu Su<sup>1,2</sup>, Lei Zu<sup>1,2,a</sup>, Yupeng Yang<sup>3,4,b</sup>, and Lei Feng<sup>1,2,4,c</sup>

<sup>1</sup> Key Laboratory of Dark Matter and Space Astronomy, Purple Mountain Observatory, Chinese Academy of Sciences, Nanjing 210023, China

<sup>2</sup> School of Astronomy and Space Science, University of Science and Technology of China, Hefei, Anhui 230026, China

<sup>3</sup> School of Physics and Physical Engineering, Qufu Normal University, Qufu, Shandong, 273165, China

<sup>4</sup> Joint Center for Particle, Nuclear Physics and Cosmology, Nanjing University–Purple Mountain Observatory, Nanjing 210093, China

Received: date / Revised version: date

**Abstract.** Observations from the James Webb Space Telescope (JWST) have unveiled several galaxies with stellar masses  $M_* \gtrsim 10^{10} M_\odot$  at redshifts  $7.4 \lesssim z \lesssim 9.1$ . These remarkable findings indicate an unexpectedly high stellar mass density, which contradicts the prediction of the  $\Lambda$ CDM model. Our study utilizes the Chevallier–Polarski–Linder (CPL) parameterization, one of the dynamic dark energy models, to probe the role of dark energy on shaping galaxy formation. By considering varying star formation efficiencies within this framework, our analysis demonstrates that in a universe with a higher proportion of dark energy, more massive galaxies are formed at high redshifts, given a fixed perturbation amplitude observed today. These intriguing results highlight the promising prospect of revealing the nature of dark energy by analyzing the high-redshift massive galaxies.

## 1 Introduction

James Webb Space Telescope (JWST) [1] has significantly enhanced our capability to explore the space regions that were previously inaccessible to the Hubble Space Telescope (HST) [2]. This remarkable achievement provides a unique opportunity to gain deeper insights into the epoch of reionization and the formation of the first galaxies [1, 3, 4]. Shortly after its commissioning, JWST has successfully identified a great number of candidate galaxies at high redshifts  $z \approx 6$ –16 [5–13], indicating that galaxies in our universe began to emit photons less than 400 million years after the Big Bang. Remarkably, the initial observations from the Cosmic Evolution Early Release Science Survey (CEERS) program unveil six candidate galaxies with stunningly high stellar masses exceeding  $10^{10} M_\odot$  at  $7.4 \lesssim z \lesssim 9.1$ , including one galaxy with a mass of approximately  $10^{11} M_\odot$  [12]. These high-redshift massive galaxies provide evidence for a star formation efficiency of  $\epsilon = 0.84$  at  $z \approx 7.5$  and  $\epsilon = 0.99$  at  $z \approx 9$  [14], potentially exceeding the cosmic baryon mass budget within collapsed structures. Although further confirmation is required for these spectroscopic observations based solely on photometry, JWST has posed a challenge to the  $\Lambda$ CDM model [14–16]. Various models have been proposed to address this issue, such as primordial black holes (PBHs) [17–19], dark matter [20–23], dark energy [24–26], and others [27–30].

Among these proposed approaches, dark energy models stand out as a potentially promising mechanism due to their simplicity and potential effectiveness.

Dark energy is introduced to drive the accelerating expansion of the universe, which is firstly supported by the observations of Type Ia supernovae (SN Ia) [31, 32]. This mysterious component also plays a significant role in shaping the evolution of the universe, especially in the formation of structures. However, its nature remains enigmatic. The cosmological constant, first proposed by Einstein, is the most concise and natural model which associates it with the energy density of the vacuum. However, recent observations suggest the possibility of the dynamical evolution of dark energy rather than  $\Lambda$ CDM model [33]. To portray this, various models have been proposed, including Quintessence [34, 35], Quintom [36], early dark energy model [37, 38] and so on [39, 40]. Usually, we use a parametric equation to describe the evolution of the dark energy equation of state (EoS), and one of the most popular choices is the Chevallier–Polarski–Linder (CPL) parameterization [41, 42]. This parameterization offers a flexible and model-independent framework to examine the evolution of the late universe.

Recently, Menci et al. [24] have adopted the CPL parameterization to discuss the tension between the JWST observations and the  $\Lambda$ CDM model. In this study, we follow the work of Menci et al. and further explore the impact of star formation efficiency on structure formation. However, our results indicate that incorporating additional dark energy within the CPL parameterization could in-

<sup>a</sup> e-mail: zulei@pmo.ac.cn (corresponding author)

<sup>b</sup> e-mail: ypyang@qfmu.edu.cn (corresponding author)

<sup>c</sup> e-mail: fenglei@pmo.ac.cn (corresponding author)

deed explain the presence of high-redshift massive galaxies observed by JWST, even with a low star formation efficiency  $\epsilon \sim 0.05$  ( $3\sigma$  confidence level), which contradicts with the results of Menci et al.

This paper is organized as follows. In Section 2, we provide a brief introduction to the CPL parameterization and the halo mass function that we adopt. We also outline the methodology for calculating the theoretical stellar mass density. In Section 3, we present the results of our analysis, focusing on the impact of the CPL parameterization with varying star formation efficiencies on the process of star formation. Additionally, we also present the constraints on the parameter space of the CPL parametrization using data from JWST. Finally, in Section 4, we summarize our findings and draw our conclusions.

## 2 Methods

### 2.1 The CPL parameterization

Although our knowledge on the nature of dark energy is currently limited, the EoS ( $w = p/\rho$ ) for dark energy can still describe its property to a certain extent. In the CPL parameterization,  $w$  is no longer a constant but varies linearly with the redshift  $z$  as

$$w(z) = w_0 + w_a \frac{z}{1+z}, \quad (1)$$

where  $w_0$  and  $w_a$  are two free parameters. The CPL parameterization will reduce to the  $\Lambda$ CDM model when  $w_0 = -1$ ,  $w_a = 0$ . It is evident that  $w(z)$  tends to  $w_0 + w_a$  in the early universe ( $z \rightarrow \infty$ ) and equates to  $w_0$  at present ( $z = 0$ ). In this parameterization, the dimensionless Hubble parameter  $E(z) = H(z)/H_0$  is

$$E^2(z) = \Omega_{\text{de}}(1+z)^{3(1+w_0+w_a)} e^{-3w_a(\frac{z}{1+z})} + \Omega_{\text{m}}(1+z)^3 + \Omega_{\text{r}}(1+z)^4, \quad (2)$$

where  $\Omega_{\text{de}}$ ,  $\Omega_{\text{m}}$  and  $\Omega_{\text{r}}$  are the fractional energy density of dark energy, dark matter and radiation, respectively. It is apparent that larger  $w_0$  and  $w_a$  correspond to more significant dark energy density and result in a larger cosmic expansion rate. All cosmological models should induce the same structure at present and the density perturbations must increase with  $w_a$  at  $z = 7 \sim 10$ . Therefore, we expect to obtain high-redshift massive galaxies through increasing  $w_a$ .

### 2.2 The halo mass function

Since luminous galaxies condense from gas within dark matter halos [43, 44], the choice of an appropriate halo mass function is crucial for accurate galaxy formation calculation. The Press–Schechter (PS) function [45], based on the spherical collapse model, has been widely used as an analytic formula for the halo mass function. However, the PS function tends to overestimate the abundance of halos

near the characteristic mass and underestimate the abundance in the high-mass tail [46–48]. To overcome this limitation, various analytical halo mass functions have been proposed to fit numerical results more accurately [48–54]. In this study, we adopt the Sheth–Tormen (ST) halo mass function [49, 50], which is based on the ellipsoidal collapse model and has been shown to enhance the accuracy of fitting  $N$ -body simulation results. The ST function is expressed as

$$f(\nu) = A \sqrt{\frac{2a}{\pi}} \left[ 1 + \left( \frac{1}{a\nu^2} \right)^p \right] \nu \exp\left(-\frac{a\nu^2}{2}\right), \quad (3)$$

where the parameters  $A = 0.3222$ ,  $p = 0.3$  and  $a = 0.707$  are determined based on simulation results. In the above equation,  $\nu = \delta_c/\sigma(M, z)$ , where  $\delta_c$  is the density threshold for spherical collapse, above which density fluctuations collapse and form a virialized halo. The critical overdensity  $\delta_c$  has a weak dependence on cosmological models, so we adopt a consistent value of  $\delta_c = 1.686$  [55] for various combinations of  $w_0$  and  $w_a$ . Additionally,  $\sigma(M, z)$  denotes the variance of the linear matter power spectrum  $P(k)$  smoothed on the scale  $R(M) = (3M/4\pi\bar{\rho})^{1/3}$  using the top-hat filter  $W(x) = 3[\sin(x) - x\cos(x)]/x^3$ , where  $\bar{\rho}$  represents the mean density of the universe at present. Altogether, the explicit expression of  $\sigma(M, z)$  is defined as

$$\sigma^2(M, z) \equiv \frac{D^2(z)}{2\pi^2} \int_0^\infty k^2 P(k) W^2(kR(M)) dk, \quad (4)$$

where  $D(z)$  denotes the linear growth factor normalized to  $D(0) = 1$ . Using the ST function, we can estimate the number density of dark matter halos. The evolution of the number density for a given mass per unit comoving volume can be described as [45, 56]:

$$\frac{dn}{dM} = f(\nu) \frac{\bar{\rho}}{M^2} \frac{d \ln \sigma^{-1}}{d \ln M}. \quad (5)$$

To compare the number density of dark matter halos between different cosmological models, it is necessary to normalize the matter power spectrum. Two main normalization methods are commonly used. The first one involves normalizing the power spectrum to match the Cosmic Microwave Background (CMB) data at redshift  $z \sim 1090$  [25, 57] with the same primordial power spectrum amplitude  $A_s$  and spectral index  $n_s$ . The second method entails normalizing the halo mass function to be consistent at  $z = 0$ . These two normalization approaches may produce differing outcomes [57]. Here, we choose to normalize the power spectrum through the second method. There are two reasons for that. Firstly, compared with the measurements of CMB anisotropy, cluster abundance measurements provide a more direct probe of density perturbation relevant to galaxy formation [58]. Secondly, normalizing the primordial power spectrum makes it challenging to distinguish the impact from different combinations of  $(w_0, w_a)$  on galaxy formation [25], as the dark energy in the CPL parameterization predominantly affects the late universe.

From Eq. (3), it is apparent that the halo mass function is uniquely affected by the cosmological model through  $\nu(z, M) = \delta_c(z)/\sigma(M, 0)D(z)$ . In our analysis, we employ the following fitting formula for  $\sigma(M, 0)$  [59]:

$$\sigma(M, 0) = \sigma_8 \left( \frac{M}{M_8} \right)^{-\gamma(M)/3}, \quad (6)$$

where  $M_8$  corresponds to the mass enclosed within a sphere of radius  $R_8 = 8h^{-1}$  Mpc, and  $\sigma_8$  is

$$\sigma_{8,\text{CPL}} = \frac{\delta_{c,\text{CPL}}(0)}{\delta_{c,\text{ACDM}}(0)} \sigma_{8,\text{ACDM}}. \quad (7)$$

Generally, different cosmological models with various parameters would yield different  $\sigma_8$ . However, since the discrepancy between  $\delta_{c,\text{CPL}}(0)$  and  $\delta_{c,\text{ACDM}}(0)$  is negligible, we can use the same  $\sigma_8$  to normalize the current value of  $f(\nu)$  [24]. In this work, we use the PYTHON package **CLASS** [60] and **COLOSSUS** to calculate the halo mass function.

### 2.3 The stellar mass density

The stellar mass  $M_*$  contained within a particular dark matter halo is expressed by the equation  $M_* = f_b M_{\text{halo}}$ , where  $M_{\text{halo}}$  is the mass of the dark matter halo, and  $f_b = \Omega_b/\Omega_m$  represents the cosmic baryon fraction, with  $\Omega_b$  being the fractional energy density of baryon. In order to fit JWST observations [12] within the CPL parameterization, we introduce the maximum cumulative stellar mass density expressed as

$$\rho_{\text{max}}(> M_*) \equiv f_b \epsilon \int_{z_1}^{z_2} \int_{M_{\text{halo}}}^{\infty} \frac{dn}{dM} M dM \frac{dV}{dz} \frac{dz}{V(z_1, z_2)}, \quad (8)$$

where  $V$  represents the comoving volume and satisfies

$$\frac{dV}{dz} = \frac{4\pi d_L^2}{H(z)(1+z)^2}, \quad (9)$$

with  $d_L$  being the luminosity distance.

Furthermore, there is another crucial physical quantity that warrants attention: the star formation efficiency, denoted by  $\epsilon$ , which represents the ratio of stellar mass to baryon mass. Previous studies ( $z \approx 0-10$ ) have shown that halos with masses near  $10^{12} M_\odot$  at redshift  $z \sim 2$  are the most efficient when forming stars, with a star formation efficiency of  $\epsilon = 0.2-0.4$  [61, 62]. While halos with much higher or lower masses, or those at higher redshift such as JWST observation ( $7.4 \lesssim z \lesssim 9.1$ ), are supposed to have lower efficiencies [61]. Recently, Boylan-Kolchin [14] has found that plausible values of  $\epsilon = 0.1$  or  $0.32$  in the  $\Lambda$ CDM model encounter challenges in explaining JWST observations. In light of these findings, our study considers three distinct star formation efficiencies:  $\epsilon = 0.1, 0.32$ , and  $0.5$ , with  $0.1$  and  $0.32$  considered plausible, while  $0.5$  is deemed extreme.

The cosmological parameters we use are as follows:  $H_0 = 67.32 \text{ km s}^{-1} \text{ Mpc}^{-1}$ ,  $\Omega_m = 0.3158$ ,  $f_b = 0.156$ ,  $n_s =$

$0.96605$ ,  $\sigma_8 = 0.8120$ ,  $100\theta_* = 1.0410$ , and  $\tau = 0.0543$ . These values are derived from the best-fit results of the Planck Collaboration for the  $\Lambda$ CDM model [63]. Due to the challenge of reconciling the JWST observations with the CMB data [25], we opt to use consistent parameters across different cosmological models as benchmark points instead of conducting a global parameter fitting based on CMB data. This approach is an approximation method, which brings a certain degree of uncertainty. In addition, although the cosmic baryon fraction  $f_b$  may vary across different scales, it is common to adopt the average value of  $f_b = 0.156$ .

## 3 Results and discussions

The theoretical maximum cumulative stellar mass density is presented in Fig. 1, with  $w_0 = -1$  fixed and  $w_a$  varied, alongside the JWST measurement [12] for the redshift bins of  $7 < z < 8.5$  and  $8.5 < z < 10$ . For a conservative star formation efficiency of  $\epsilon = 0.1$ , neither the  $\Lambda$ CDM model nor the CPL parameterization with fixed  $w_0 = -1$  can provide a satisfactory explanation for the JWST observations, even when  $w_a$  as large as  $0.8$ . Similarly, when considering a plausible star formation efficiency of  $\epsilon = 0.32$ , it is also struggling to account for the JWST observations within the  $\Lambda$ CDM framework. However, by selecting appropriate  $w_a$  in the CPL parameterization, the corresponding stellar mass density can be consistent with the JWST measurement when  $\epsilon = 0.32$ . For  $\epsilon = 0.5$ , the stellar mass density agrees with the observations for both the  $\Lambda$ CDM model and the CPL parameterization, with almost all the selected values of  $w_a$ . Nevertheless, a star formation efficiency of  $\epsilon = 0.5$  (i.e. half of the gas has been converted into stars) contradicts the multi-band observations [61, 62]. In summary, the results indicate that higher star formation efficiency  $\epsilon$  and larger values of  $w_a$  lead to more massive galaxies at high redshifts.

To find the optimal values of  $w_0$  and  $w_a$  in explaining the JWST observations, we compute  $\chi^2$  by scanning a two-dimensional grid ( $w_a-w_0$ ) consisting of  $100 \times 100$  points. The  $\chi^2$  is constructed as  $\chi^2(w_0, w_a) = \sum_1^i ((\rho_{\text{max},i}(w_0, w_a) - \rho_{\text{obs},i})/\sigma_i)^2$ , where  $\rho_{\text{max},i}(w_0, w_a)$  is the theoretical maximum of the cumulative stellar mass density, the observed density  $\rho_{\text{obs},i}$  and error bars  $\sigma_i$  are obtained from Ref. [12] shown as the five blue points in Fig. 1. After scanning the grid, we identify  $\chi_{\text{min}}^2$ . We assume the degrees of freedom to be approximately 3, although potential correlations between the observed density  $\rho_{\text{obs}}$  may result in an effective degree of freedom of less than 3. Through consulting a relevant statistical table or using software, we obtain  $\chi_{1\sigma}^2 = \chi_{\text{min}}^2 + 3.526$  ( $\chi_{2\sigma}^2 = \chi_{\text{min}}^2 + 8.02$ ) to determine  $1\sigma$  ( $2\sigma$ ) confidence region.

Under the assumption of the  $\Lambda$ CDM cosmology [12], the galaxies are found by JWST within a cosmic volume by integrating over the redshift range. Hence, it is necessary to correct the observed density  $\rho_{\text{obs},i}$  with a volume factor  $V_\Lambda/V_{w_0, w_a}$ , where  $V_\Lambda$  and  $V_{w_0, w_a}$  are the cosmic volume in the  $\Lambda$ CDM model and CPL parameterization, respectively [24, 64]. Similarly, the luminosity factor

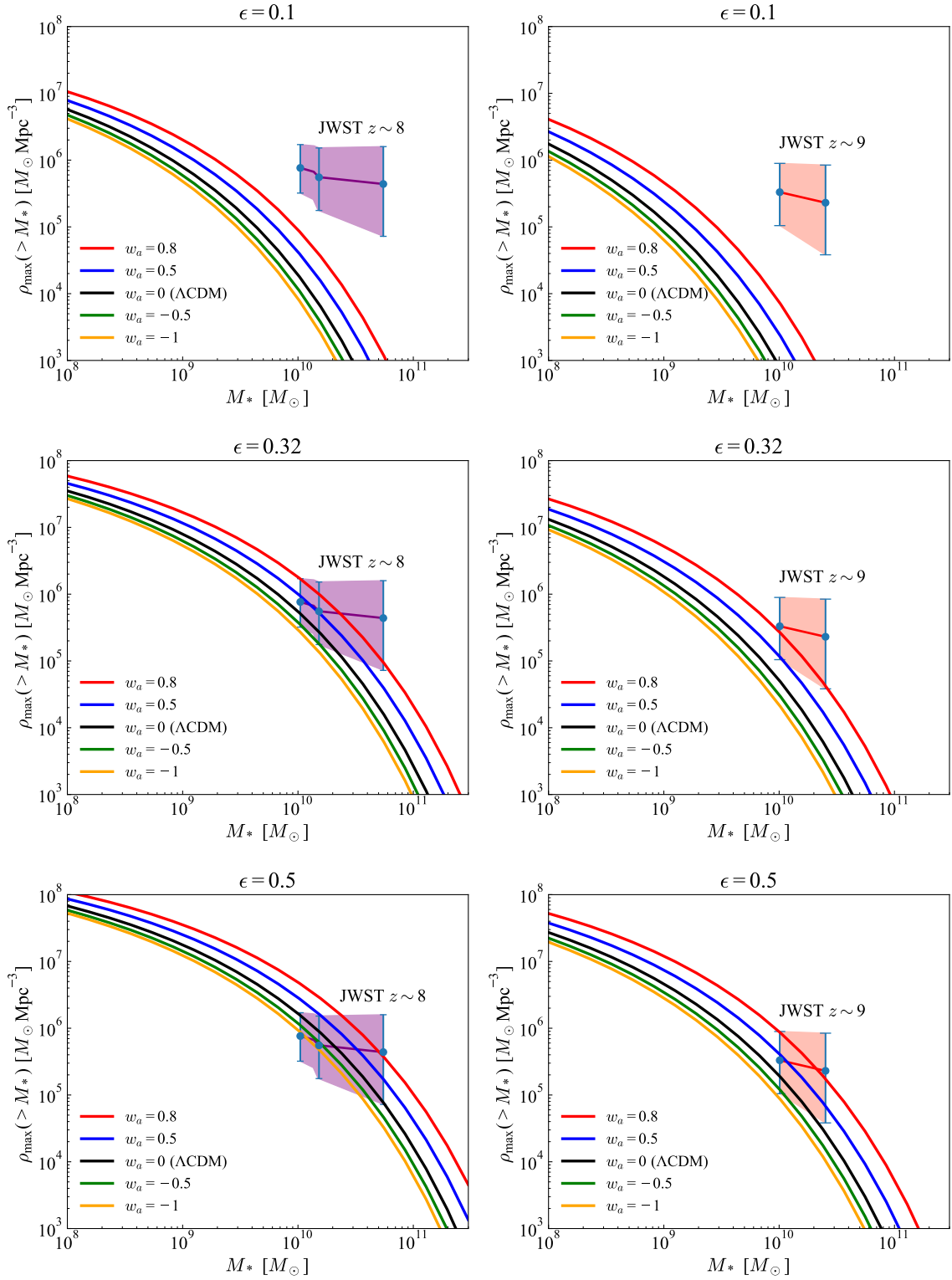


**Fig. 1.** The theoretical maximum cumulative stellar mass densities comparing with JWST observations. The CPL parameterization is applied using a fixed value of  $w_0 = -1$  along with five different values of  $w_a$ . Solid lines depict the stellar mass density of galaxies with masses exceeding  $M_*$  within two redshift bins,  $7 < z < 8.5$  (left panel) and  $8.5 < z < 10$  (right panel). For each redshift bin, three different values of star formation efficiency  $\epsilon$  are selected for analysis. The purple and red blocks illustrate the stellar mass density within the two redshift bins,  $7 < z < 8.5$  and  $8.5 < z < 10$ , respectively, based on the six massive galaxies observed by JWST [12].

$d_{L,w_0,w_a}^2/d_{L,\Lambda}^2$  is applied to correct  $\rho_{\text{obs},i}(> M_{*,i})$  and  $M_{*,i}$ , where  $d_{L,\Lambda}^2$  and  $d_{L,w_0,w_a}^2$  represent the luminosity distance in the  $\Lambda$ CDM model and CPL parameterization, respectively. Here  $z = 7.5$  and  $9.1$  are picked to represent the two redshift bins mentioned above.

The favored parameter space of  $w_a$ - $w_0$  obtained by fitting JWST data (red regions) is presented in Fig. 2. For comparison, the constraints from the CMB and Weak Lensing data (green regions), and the Hubble diagram of quasars (QSO) and SN Ia (blue regions), all sourced from Ref. [65], are also displayed in Fig. 2. We explore three distinct star formation efficiencies:  $\epsilon = 0.1, 0.32$  and  $0.5$ . In our work, we only consider the case of  $w(z) < 0$  for the reason that dark energy behaved similarly to matter or radiation in the early universe when  $w(z) \geq 0$ . Additionally, the scenario of  $w_0 < -1/(1 - \Omega_m)$  within the CPL parameterization may also be considered unphysical, as it could lead to a turning point in  $H(z)$ , which is regarded as an exotic feature in cosmology [66]. With a conservative value of  $\epsilon = 0.1$ , the parameters favored by JWST data have effectively ruled out by other cosmological observations. For  $\epsilon = 0.32$ , the JWST observations have excluded a significant portion of the parameter space for the CPL parameterization. However, there are still small regions of parameter space consistent with other observed cosmological observations. Nevertheless, for  $\epsilon = 0.5$ , it is noteworthy that there is a large parameter space that can simultaneously interpret JWST and other cosmological observations.

Based solely upon the JWST observations, the  $\chi^2$  distribution of the star formation efficiency  $\epsilon$  is presented for both the  $\Lambda$ CDM model and the CPL parameterization, as depicted in Fig. 3. It becomes evident that the  $\Lambda$ CDM model faces challenges in reconciling with the JWST observations, primarily due to its demand for an impractical star formation efficiency  $\epsilon$ , surpassing the upper limit of  $\epsilon \approx 0.2$ - $0.4$  based on previous studies [61, 62]. However, as shown in Fig. 3, the distribution of  $\chi^2$  in the CPL parameterization demonstrates a lower limit of  $\epsilon = 0.05$  at a  $3\sigma$  confidence level. This finding indicates that the CPL parameterization allows for lower star formation efficiencies compared to the  $\Lambda$ CDM model, making it a more feasible and statistically supported model in light of the JWST data.

To assess the credibility of the ST halo mass function within the  $\Lambda$ CDM model framework, we explore the impact of various halo mass function models on theoretical stellar mass density. The results are illustrated in Fig. 4, with  $\epsilon = 0.32$  adopted. In this investigation, we mainly examine four well-fitting models: ST function [49], Warren 2006 [51], Watson 2013 [52], and Despali 2016 [54]. The PS function [45] is also included, although it diverges from the detailed results of N-body simulation. Our findings reveal that the four well-fitting models exhibit very similar behaviors, whereas the PS function deviates to some extent. Consequently, we conclude that the stellar mass density shows little sensitivity to the various well-fitting halo mass function models. Based on the above, it is con-

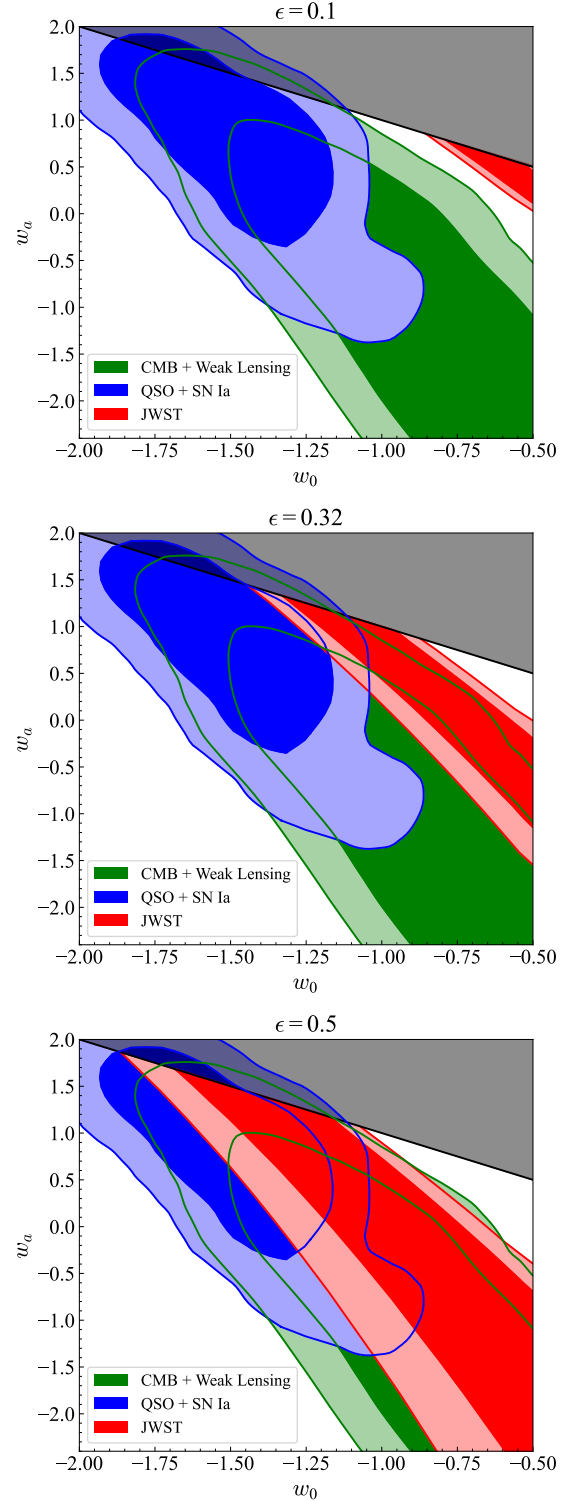


**Fig. 2.** The  $w_a$ - $w_0$  probability contours for three different choices of star formation efficiency  $\epsilon$ . The red regions represent the  $1\sigma$  and  $2\sigma$  confidence level by fitting the JWST data [12], in comparison with the  $2\sigma$  and  $3\sigma$  contours derived from CMB and Weak Lensing data (green regions) [65], and the Hubble diagram of QSO and SN Ia (blue regions) [65]. The black region denotes the excluded region satisfying  $w(z \rightarrow \infty) \approx w_0 + w_a > 0$ .

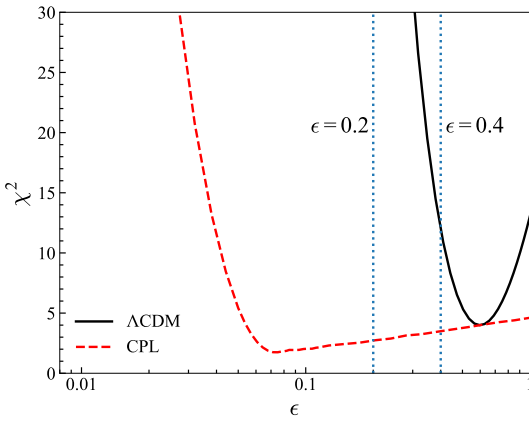


**Fig. 3.** The one-dimensional  $\chi^2$  distribution of star formation efficiency  $\epsilon$  in the  $\Lambda$ CDM model and CPL parameterization. Notably, in the case of CPL parameterization, we have adopted the minimum value of  $\chi^2$  by adjusting  $w_0$  and  $w_a$ . The blue dot lines represent the maximum star formation efficiency based on multi-band observations with a value of  $0.2 \sim 0.4$  [61, 62].

sidered credible to adopt the ST halo mass function as a representative.

### 4 Conclusions

The detection of high-redshift massive galaxies by JWST poses a significant challenge to the  $\Lambda$ CDM model. To reconcile the  $\Lambda$ CDM model with JWST observations, the star formation efficiency should be extremely high [24]. Nevertheless, when we solely consider the JWST observations, the CPL parameterization can give a successful explanation even with a low star formation efficiencies of  $\epsilon \sim 0.05$ . Our findings also indicate that, for a fixed power spectrum normalization (fixed  $\sigma_8$ ), larger values of the CPL parameter  $w_a$ , which correspond to a greater amount of dark energy, result in higher halo mass densities and more massive galaxies at high redshifts [58]. Moreover, the constraints of CPL parameters derived from JWST are consistent with other cosmological observations for large star formation efficiency.

Futhermore, due to the potential tension between CMB data and JWST observations [25, 64], we have not incorporated CMB data in the comprehensive fitting process when interpreting the JWST observations. However, it is crucial for future research to address this issue and combine JWST observations with CMB data to achieve more precise constraints on the parameter space through global fitting.

**Acknowledgements** We are grateful to Professor Xiaodong Li, Yi Wang, Yi-Zhong Fan, Yue-Lin Sming Tsai, Deng Wang for their helpful discussion. This work is supported by the National Key R&D Program of China (Grants No. 2022YFF0503304), the National Natural Science Foundation of China (12220101003, 11773075), and the Shandong Provincial Natural Science Foundation (Grant No. ZR2021MA021).

**Data Availability Statement** No Data associated in the manuscript.

### References

1. Gardner, J. P. *et al.* The James Webb Space Telescope. *Space Sci. Rev.* **123**, 485 (2006).
2. Freedman, W. L. *et al.* Final results from the hubble space telescope key project to measure the hubble constant. *The Astrophysical Journal* **553**, 47 (2001).
3. Robertson, B. E. Galaxy formation and reionization: key unknowns and expected breakthroughs by the james webb space telescope. *Annual Review of Astronomy and Astrophysics* **60**, 121–158 (2022).
4. Muñoz, J. B., Mirocha, J., Furlanetto, S. & Sabti, N. Breaking degeneracies in the first galaxies with clustering. *arXiv preprint arXiv:2306.09403* (2023).
5. Finkelstein, S. L. *et al.* A long time ago in a galaxy far, far away: A candidate  $z \sim 12$  galaxy in early JWST CEERS imaging. *The Astrophysical journal letters* **940**, L55 (2022).
6. Naidu, R. P. *et al.* Two remarkably luminous galaxy candidates at  $z \approx 10 - 12$  revealed by JWST. *The Astrophysical Journal Letters* **940**, L14 (2022).
7. Castellano, M. *et al.* Early results from GLASS-JWST. III. galaxy candidates at  $z \sim 9 - 15$ . *The Astrophysical Journal Letters* **938**, L15 (2022).
8. Yan, H., Ma, Z., Ling, C., Cheng, C. & Huang, J.-S. First batch of  $z \approx 11 - 20$  candidate objects revealed by the james webb space telescope early release observations on smacs 0723-73. *The Astrophysical Journal Letters* **942**, L9 (2022).
9. Donnan, C. *et al.* The evolution of the galaxy UV luminosity function at redshifts  $z \approx 8 - 15$  from deep JWST and ground-based near-infrared imaging. *Monthly Notices of the Royal Astronomical Society* **518**, 6011–6040 (2023).
10. Atek, H. *et al.* Revealing galaxy candidates out to  $z \sim 16$  with JWST observations of the lensing cluster SMACS0723. *Monthly Notices of the Royal Astronomical Society* **519**, 1201–1220 (2023).
11. Adams, N. *et al.* Discovery and properties of ultra-high redshift galaxies ( $9 < z < 12$ ) in the JWST ERO SMACS 0723 field. *Monthly Notices of the Royal Astronomical Society* **518**, 4755–4766 (2023).
12. Labbé, I. *et al.* A population of red candidate massive galaxies  $\sim 600$  Myr after the Big Bang. *Nature* 1–2 (2023).
13. Rodighiero, G. *et al.* JWST unveils heavily obscured (active and passive) sources up to  $z \sim 13$ . *Monthly Notices of the Royal Astronomical Society: Letters* **518**, L19–L24 (2023).
14. Boylan-Kolchin, M. Stress testing  $\Lambda$ CDM with high-redshift galaxy candidates. *arXiv preprint arXiv:2208.01611* (2022).
15. Haslbauer, M., Kroupa, P., Zonoozi, A. H. & Haghi, H. Has jwst already falsified dark-matter-driven galaxy formation? *The Astrophysical Journal Letters* **939**, L31 (2022).
16. Lovell, C. C., Harrison, I., Harikane, Y., Tacchella, S. & Wilkins, S. M. Extreme value statistics of the halo and stellar mass distributions at high redshift: are JWST results in tension with  $\Lambda$ CDM? *Monthly Notices of the Royal Astronomical Society* **518**, 2511–2520 (2023).

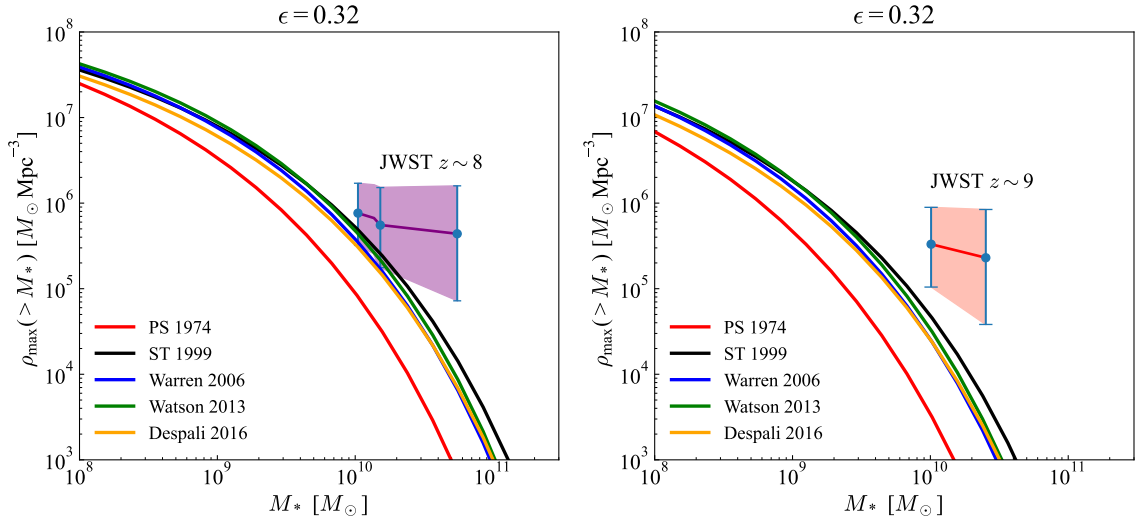


**Fig. 4.** The theoretical maximum cumulative stellar mass densities with various halo mass functions. Similar to Fig. 1. However, we employed different halo mass functions, including PS 1974 [45], ST 1999 [49], Warren 2006 [51], Watson 2013 [52], and Despali 2016 [54], to examine their influence on the theoretical stellar mass densities in the  $\Lambda$ CDM model, with  $\epsilon = 0.32$  fixed.

17. Liu, B. & Bromm, V. Accelerating early massive galaxy formation with primordial black holes. *The Astrophysical Journal Letters* **937**, L30 (2022).
18. Yuan, G.-W. *et al.* Rapidly growing primordial black holes as seeds of the massive high-redshift JWST galaxies. *arXiv preprint arXiv:2303.09391* (2023).
19. Su, B.-Y., Li, N. & Feng, L. An inflation model for massive primordial black holes to interpret the jwst observations. *arXiv preprint arXiv:2306.05364* (2023).
20. Gong, Y., Yue, B., Cao, Y. & Chen, X. Fuzzy dark matter as a solution to the stellar mass density of high- $z$  massive galaxies. *arXiv preprint arXiv:2209.13757* (2022).
21. Dayal, P. & Giri, S. K. Warm dark matter constraints from the jwst. *arXiv preprint arXiv:2303.14239* (2023).
22. Hütsi, G., Raidal, M., Urrutia, J., Vaskonen, V. & Veermäe, H. Did JWST observe imprints of axion mini-clusters or primordial black holes? *Physical Review D* **107**, 043502 (2023).
23. Lin, H., Gong, Y., Yue, B. & Chen, X. Implications of the stellar mass density of high- $z$  massive galaxies from jwst on warm dark matter. *arXiv preprint arXiv:2306.05648* (2023).
24. Menci, N. *et al.* High-redshift galaxies from early JWST observations: Constraints on dark energy models. *The Astrophysical Journal Letters* **938**, L5 (2022).
25. Wang, D. & Liu, Y. JWST high redshift galaxy observations have a strong tension with Planck CMB measurements. *arXiv preprint arXiv:2301.00347* (2023).
26. Klypin, A. *et al.* Clustering and halo abundances in early dark energy cosmological models. *Monthly Notices of the Royal Astronomical Society* **504**, 769–781 (2021).
27. Biagetti, M., Franciolini, G. & Riotto, A. High-redshift JWST observations and primordial non-gaussianity. *The Astrophysical Journal* **944**, 113 (2023).
28. Parashari, P. & Laha, R. Primordial power spectrum in light of jwst observations of high redshift galaxies. *arXiv preprint arXiv:2305.00999* (2023).
29. Wang, Y.-Y., Lei, L., Yuan, G.-W. & Fan, Y.-Z. Modeling the JWST High-redshift Galaxies with a General Formation Scenario and the Consistency with the  $\Lambda$ CDM Model. *Astrophys. J. Lett.* **954**, L48 (2023).
30. Jiao, H., Brandenberger, R. & Refregier, A. Early structure formation from cosmic string loops in light of early jwst observations. *arXiv preprint arXiv:2304.06429* (2023).
31. Riess, A. G. *et al.* Observational evidence from supernovae for an accelerating universe and a cosmological constant. *The astronomical journal* **116**, 1009 (1998).
32. Perlmutter, S. *et al.* Measurements of  $\Omega$  and  $\Lambda$  from 42 high-redshift supernovae. *The Astrophysical Journal* **517**, 565 (1999).
33. Zhao, G.-B. *et al.* Dynamical dark energy in light of the latest observations. *Nature Astronomy* **1**, 627–632 (2017).
34. Amendola, L. Coupled quintessence. *Physical Review D* **62**, 043511 (2000).
35. Banerjee, A. *et al.* Hubble sinks in the low-redshift swampland. *Physical Review D* **103**, L081305 (2021).
36. Caldwell, R. R. A phantom menace? cosmological consequences of a dark energy component with super-negative equation of state. *Physics Letters B* **545**, 23–29 (2002).
37. Doran, M. & Robbers, G. Early dark energy cosmologies. *Journal of Cosmology and Astroparticle Physics* **2006**, 026 (2006).
38. Poulin, V., Smith, T. L., Karwal, T. & Kamionkowski, M. Early dark energy can resolve the hubble tension. *Physical review letters* **122**, 221301 (2019).
39. Li, M. A model of holographic dark energy. *Physics Letters B* **603**, 1–5 (2004).
40. Feng, L. & Lu, T. A new equation of state for dark energy model. *JCAP* **11**, 034 (2011).
41. Chevallier, M. & Polarski, D. Accelerating universes with scaling dark matter. *International Journal of Modern Physics D* **10**, 213–223 (2001).
42. Linder, E. V. Exploring the expansion history of the universe. *Physical review letters* **90**, 091301 (2003).
43. White, S. D. & Rees, M. J. Core condensation in heavy halos: a two-stage theory for galaxy formation and clustering. *Monthly Notices of the Royal Astronomical Society* **183**, 341–358 (1978).

44. Somerville, R. S. & Primack, J. R. Semi-analytic modelling of galaxy formation: the local universe. *Monthly Notices of the Royal Astronomical Society* **310**, 1087–1110 (1999).
45. Press, W. H. & Schechter, P. Formation of galaxies and clusters of galaxies by self-similar gravitational condensation. *The Astrophysical Journal* **187**, 425–438 (1974).
46. Efstathiou, G., Frenk, C. S., White, S. D. & Davis, M. Gravitational clustering from scale-free initial conditions. *Monthly Notices of the Royal Astronomical Society (ISSN 0035-8711)*, vol. 235, Dec. 1, 1988, p. 715–748. *Research supported by the Nuffield Foundation and SERC*. **235**, 715–748 (1988).
47. Lacey, C. & Cole, S. Merger rates in hierarchical models of galaxy formation—ii. comparison with n-body simulations. *Monthly Notices of the Royal Astronomical Society* **271**, 676–692 (1994).
48. Jenkins, A. *et al.* The mass function of dark matter haloes. *Monthly Notices of the Royal Astronomical Society* **321**, 372–384 (2001).
49. Sheth, R. K. & Tormen, G. Large-scale bias and the peak background split. *Monthly Notices of the Royal Astronomical Society* **308**, 119–126 (1999).
50. Sheth, R. K., Mo, H. & Tormen, G. Ellipsoidal collapse and an improved model for the number and spatial distribution of dark matter haloes. *Monthly Notices of the Royal Astronomical Society* **323**, 1–12 (2001).
51. Warren, M. S., Abazajian, K., Holz, D. E. & Teodoro, L. Precision determination of the mass function of dark matter halos. *The Astrophysical Journal* **646**, 881 (2006).
52. Watson, W. A. *et al.* The halo mass function through the cosmic ages. *Monthly Notices of the Royal Astronomical Society* **433**, 1230–1245 (2013).
53. Tinker, J. *et al.* Toward a halo mass function for precision cosmology: The limits of universality. *The Astrophysical Journal* **688**, 709 (2008).
54. Despali, G. *et al.* The universality of the virial halo mass function and models for non-universality of other halo definitions. *Monthly Notices of the Royal Astronomical Society* **456**, 2486–2504 (2016).
55. Gunn, J. E. & Gott III, J. R. On the infall of matter into clusters of galaxies and some effects on their evolution. *The Astrophysical Journal* **176**, 1 (1972).
56. Bond, J., Cole, S., Efstathiou, G. & Kaiser, N. Excursion set mass functions for hierarchical gaussian fluctuations. *The Astrophysical Journal* **379**, 440–460 (1991).
57. Mortonson, M. J., Hu, W. & Huterer, D. Simultaneous falsification of  $\Lambda$ CDM and quintessence with massive, distant clusters. *Physical Review D* **83**, 023015 (2011).
58. Kuhlen, M., Strigari, L. E., Zentner, A. R., Bullock, J. S. & Primack, J. R. Dark energy and dark matter haloes. *Monthly Notices of the Royal Astronomical Society* **357**, 387–400 (2005).
59. VianaPedro, T. & Liddle, A. R. The cluster abundance in flat and open cosmologies. *Monthly Notices of the Royal Astronomical Society* **281**, 323–332 (1996).
60. Blas, D., Lesgourgues, J. & Tram, T. The cosmic linear anisotropy solving system (CLASS). Part II: approximation schemes. *Journal of Cosmology and Astroparticle Physics* **2011**, 034 (2011).
61. Behroozi, P. S., Wechsler, R. H. & Conroy, C. The average star formation histories of galaxies in dark matter halos from  $z=0-8$ . *The Astrophysical Journal* **770**, 57 (2013).
62. Behroozi, P., Wechsler, R. H., Hearin, A. P. & Conroy, C. Universe-machine: The correlation between galaxy growth and dark matter halo assembly from  $z=0-10$ . *Monthly Notices of the Royal Astronomical Society* **488**, 3143–3194 (2019).
63. Aghanim, N. *et al.* Planck 2018 results-VI. Cosmological parameters. *Astronomy & Astrophysics* **641**, A6 (2020).
64. Forconi, M., Melchiorri, A., Mena, O., Menci, N. *et al.* Do the early galaxies observed by jwst disagree with planck’s cmb polarization measurements? *arXiv preprint arXiv:2306.07781* (2023).
65. Risaliti, G. & Lusso, E. Cosmological constraints from the hubble diagram of quasars at high redshifts. *Nature Astronomy* **3**, 272–277 (2019).
66. Colgáin, E. Ó. & Sheikh-Jabbari, M. A critique of holographic dark energy. *Classical and Quantum Gravity* **38**, 177001 (2021).